Letter

Doping fingerprints of spin and lattice fluctuations in moiré superlattice systems

Niklas Witt [1,2,3,*] José M. Pizarro [1,4,†] Jan Berges [1] Takuya Nomoto [5] Ryotaro Arita [5,6] and Tim O. Wehling [1,2,3,‡]

[1]*Institute of Theoretical Physics, Bremen Center for Computational Materials Science, and MAPEX Center for Materials and Processes, University of Bremen, Otto-Hahn-Allee 1, 28359 Bremen, Germany*

[2]*I. Institute of Theoretical Physics, University of Hamburg, Notkestraße 9, 22607 Hamburg, Germany*

[3]*The Hamburg Centre for Ultrafast Imaging, Luruper Chaussee 149, 22761, Hamburg, Germany*

[4]*Max Planck Institute for the Structure and Dynamics of Matter, Luruper Chaussee 149, 22671 Hamburg, Germany*

[5]*Department of Applied Physics, The University of Tokyo, 7-3-1 Hongo, Bunkyo-ku, Tokyo 113-8656, Japan*

[6]*RIKEN Center for Emergent Matter Science, 2-1 Hirosawa, Wako, Saitama 351-0198, Japan*

(Received 12 August 2021; revised 18 March 2022; accepted 26 May 2022; published 13 June 2022)

Twisted Van der Waals systems offer the unprecedented possibility to tune different states of correlated quantum matter with external noninvasive electrostatic doping. The nature of the superconducting order presents a recurring open question in this context. In this work, we assess quantitatively the case of spin-fluctuation-mediated pairing for Γ-valley twisted transition metal dichalcogenide homobilayers. We calculate self-consistently and dynamically the doping-dependent superconducting transition temperature T_c revealing a superconducting dome with a maximal $T_c \approx 0.1$–1 K depending on twist angle. We compare our results with conventional phonon-mediated superconductivity, and we identify clear fingerprints in the doping dependence of T_c, which enable experiments to distinguish between different pairing mechanisms.

DOI: 10.1103/PhysRevB.105.L241109

Introduction. Twisting layers of two-dimensional (2D) materials leads to a moiré pattern, where flat bands can emerge close to the Fermi level [1–3]. The associated quenching of the kinetic energy leads to strong electronic correlations, which often interplay with topology [4–6]. Among these effects are Mott and topological Chern insulators, and different kinds of magnetic, nematic, and superconducting ordered states [7–28]. One can precisely tune between these states and change the filling of the flat bands from completely empty to filled by electrostatic doping [29], which is special in the domain of correlated materials.

The nature of superconducting states in twisted 2D systems is highly controversial. On the one hand, unconventional pairing mechanisms based on spin, orbital, and/or nematic fluctuations are regularly hypothesized [27,30–34]. The reasons are that superconductivity emerges next to a strongly correlated state [8,9,20,27,35] and that the ratio of critical temperature T_c and Fermi temperature T_F fits within the boundary of other unconventional superconductors [8,24,36]. On the other hand, recent experiments in magic-angle twisted bilayer graphene (MATBG) showed that the strongly correlated states and superconductivity are affected differently by the dielectric environment [17,18,28], which might point to a conventional origin, i.e., electron-phonon coupling.

Twisted 2D systems can be classified according to the symmetry of the low-energy Hamiltonian associated with the moiré pattern [37]. Honeycomb twisted 2D systems hold promise for hosting correlated Dirac fermions and topological $d + id$ chiral superconductivity [30,38,39]. Examples of honeycomb systems are MATBG [3,40], twisted double bilayer graphene [41–43], magic-angle twisted trilayer graphene (MATTG) [44–46], and twisted transition metal dichalcogenides (TMDCs) [47–49]. Most of the experimental and theoretical work has been focused on graphite-based systems. However, their complicated low-energy electronic structure makes theoretical many-body studies difficult [42–46,50–52]. The low-energy electronic structure of twisted TMDC homobilayers is simpler than that of twisted graphitic systems since it can be described by an effective single-orbital model (see below) and it does not show topological obstruction preventing simple Wannier constructions [40,53]. As such, they are good candidates for establishing a link between experiments and theoretical many-body modeling. Recently, a zero-resistance state has been reported in a twisted TMDC homobilayer [20], the nature of which remains to be understood.

In this Letter we provide a quantitative study of the critical temperature T_c due to spin-fluctuation-mediated pairing in Γ-valley twisted TMDCs in terms of doping and twisting, which we obtain dynamically by means of the fluctuation exchange approximation (FLEX) [54,55]. We additionally provide a qualitative understanding of spin fluctuations versus electron-phonon coupling, and we propose that experimental measurements on the doping-dependent T_c can help to unveil the nature of the superconducting states.

Band Structures, Wannierization and Hartree Potential Effect. We consider the twisting of TMDC homobilayers with respect to the untwisted ($\theta = 0^\circ$) situation. In Fig. 1(a) we show the emergent moiré pattern, where the AA regions form a triangular superlattice surrounded by AB and BA regions arranged in a honeycomb pattern. We focus on the so-called Γ-valley twisted TMDCs (WS_2, MoS_2, and $MoSe_2$)

*niklas.witt@physik.uni-hamburg.de
†jose.pizarro@mpsd.mpg.de
‡tim.wehling@physik.uni-hamburg.de

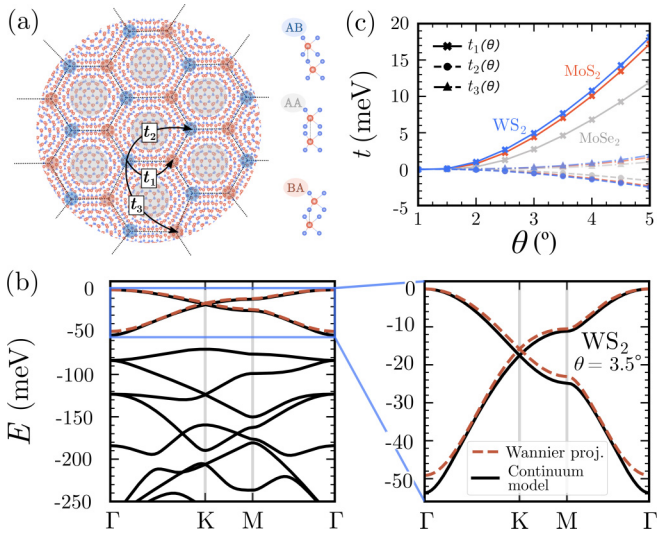

FIG. 1. Γ-valley twisted TMDCs. (a) Moiré pattern of twisted TMDCs. AA (gray shaded), AB (blue shaded), and BA (red shaded) regions in the moiré pattern correspond to different stackings of the two layers, as shown on the right side. Dashed black lines serve as a guide to the eye to identify the honeycomb superlattice. The most relevant hopping processes are sketched with black arrows. (b) Continuum model for WS_2 at a twist angle of $\theta = 3.5°$ (black solid line) with a third-nearest-neighbor hopping tight-binding model (red dashed line) of the highest valence bands. The effective honeycomb lattice is formed by the AB and BA moiré sites. The right panel shows a zoom of the flat Dirac bands. (c) Twist-angle dependence of the hopping parameters for different Γ-valley twisted TMDCs, WS_2, MoS_2, and $MoSe_2$ obtained via Wannier projection.

[49,56,57], in which the valence band maximum of the untwisted homobilayer is located at the center of the Brillouin zone Γ due to the hybridization between the transition metal d and chalcogen p orbitals. The valence band maximum is an antibonding state energetically separated from its bonding counterpart by hundreds of meV. Also the conduction band is separated from the valence band maximum by more than an eV [58,59]. Based on this observation, Angeli and MacDonald constructed a low-energy continuum model in which only the antibonding state is included [49]. The emergent symmetry of these moiré valence bands is that of a 2D honeycomb lattice.

In the plane-wave basis defined by the moiré vectors $\mathbf{G} = m\mathbf{G}_1^{\mathrm{M}} + n\mathbf{G}_2^{\mathrm{M}}$, with integers m, n and $\mathbf{G}_{1,2}^{\mathrm{M}}$ spanning the reciprocal lattice, the Hamiltonian of the continuum model takes the form

$$H = -\frac{\hbar^2|\mathbf{k}+\mathbf{G}|^2}{2m^*}\delta_{\mathbf{G},\mathbf{G}'} + V_{\mathrm{M}}(\mathbf{G}-\mathbf{G}'), \qquad (1)$$

where $\mathbf{k}$ are the reciprocal vectors defined in the mini Brillouin zone, m^* is the effective mass, and $V_{\mathrm{M}}(\mathbf{G})$ is the Fourier transformation of the moiré potential [60]. This Hamiltonian is expanded up to a plane-wave cutoff $G_{\mathrm{c}} = 5G^{\mathrm{M}}$, where $G^{\mathrm{M}} = |\mathbf{G}_{1,2}^{\mathrm{M}}|$.

The low-energy electronic structure of Γ-valley twisted TMDCs shows 2D honeycomb Dirac bands for the highest valence band; see Fig. 1(b). The Dirac point can be accessed by hole doping and the Dirac bands are well isolated from higher energy bands for twist angles $1° < \theta < 5°$. In this twist angle range, the bandwidth of the flat Dirac bands varies between 0.5 and 100 meV [60].

We next construct a tight-binding Hamiltonian to describe the flat Dirac bands with one orbital per honeycomb superlattice site. Here, the AB and BA regions play the role of the A and B sublattice degrees of freedom in the honeycomb lattice. We include up to three nearest-neighbor hoppings t_1, t_2, t_3 in our model, which we obtain by Wannier projection [60]. The tight-binding and continuum model band structure agree very well in the twist angle range $1° < \theta < 5°$ [60]. We observe that, when comparing among different Γ-valley twisted TMDCs, the transition metal does not influence the hopping amplitudes significantly, while the chalcogen atoms do. We also find dominant nearest-neighbor hopping $t_1 \gg t_2, t_3$, and that $t_1 \sim \alpha \sin^2(\theta) \approx \alpha\theta^2$ with $\alpha \approx 2$ eV/rad^2.

In other twisted 2D systems, such as MATBG [61–64] or MATTG [34], the effect of the purely electrostatic and long-range (Hartree) potential in doped flat bands is important. Thus, we also consider its influence in our model [60]. We find that, contrary to MATBG and MATTG, the flat Dirac bands remain unaffected. Therefore, we disregard doping-dependent long-range Coulomb reconstructions on the flat bands from now on.

Doping- and Interaction-dependent Spin Fluctuations. Since the nearest-neighbor hopping $t_1(\theta)$ dominates over t_2 and t_3 for twist angles $1° < \theta < 5°$, we neglect t_2 and t_3 here. We discuss their influence in the Supplemental Material [60]. We study the Hubbard Hamiltonian

$$H_U = -\sum_{\langle im,jn\rangle,\sigma} t(c_{im\sigma}^\dagger c_{jn\sigma} + \mathrm{H.c.}) + U\sum_{im} n_{im\uparrow}n_{im\downarrow}, \qquad (2)$$

where the hopping amplitude $t \equiv t_1(\theta)$ sets the energy scale, and $\langle im, jn\rangle$ denotes that the sum is limited to neighboring lattice sites of a moiré unit cell i, j and sublattice m, n. $c_{im\sigma}^\dagger$ ($c_{im\sigma}$) creates (annihilates) an electron with spin σ, and U is the local Coulomb repulsion between electrons on the same lattice site. In the simplified tight-binding model, the system is particle-hole symmetric with respect to the Dirac point and has a logarithmically diverging density of states (DOS) at the Van Hove singularities (VHS) that are present in the M points of the Brillouin zone [65]. We redefine our zero-doping level $\delta = 0$ to correspond to a Fermi energy at the Dirac point; see Fig. 1(b). Then, the VHS are at $\delta = 0.25$.

The Hubbard model for the honeycomb lattice has previously been studied, indicating a rich phase diagram of competing many-body instabilities [39,66–72]. The emergence of spin-density waves (SDWs) and superconductivity in close proximity suggests an unconventional pairing mechanism mediated by spin fluctuations. Following this premise, we study the magnetic and superconducting excitations using FLEX [60] in the model described above [73–75] as a representation of spin-fluctuation-mediated pairing in Γ-valley twisted TMDCs. A recently developed sparse sampling method [76,77] enabled us to perform the numerically demanding calculations at low temperatures.

In FLEX, the exchange of spin and charge fluctuations is treated dynamically and self-consistently with an effective electron-electron interaction of a random phase approximation (RPA) type. Estimates of the Hubbard interaction

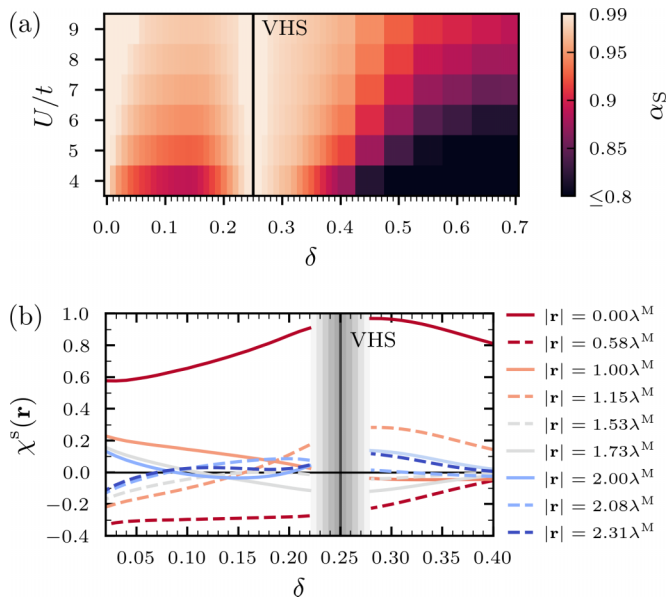

FIG. 2. Spin fluctuation characteristics of Γ-valley twisted TMDCs at $T/t = 0.003$. (a) Leading Stoner enhancement factor $\alpha_S = \max_{\mathbf{q}}\{U\chi^0(\mathbf{q})\}$ for different Coulomb interaction strengths U/t and dopings δ with respect to the Dirac point as obtained from FLEX. A transition to a quasiordered magnetic state is assumed for $\alpha_S \geqslant 0.99$. (b) Real-space components of the static spin susceptibility $\chi^s(\mathbf{r})$ for $U/t = 6$. Up to eighth-nearest-neighbor components are shown, with $|\mathbf{r}|$ denoting the distance between two spins in terms of the moiré unit length λ^M. Solid (dashed) lines correspond to the AA (AB) components of χ^s, i.e., correlations between same (different) sublattice sites. The area around the Van Hove singularities (VHS) is not accessible because of too strong fluctuations; it is marked by a gray shaded area [cf. panel (a)].

parameter given in the Supplemental Material [60] show that U is highly tunable via twist angle and the dielectric environment [17,18,28,78–84]. For example, for $\theta = 5°$, the interaction strength is tunable in the range $4 < U/t < 8$ [60]. In addition, vertex corrections that are neglected in FLEX could contribute to further screening [85–87]. In what follows, we treat U as a free parameter.

We analyze the emergence of magnetic fluctuations by inspecting the leading Stoner enhancement factor $\alpha_S = \max_{\mathbf{q}}\{U\chi^0(\mathbf{q})\}$ with the static irreducible susceptibility $\chi^0(\mathbf{q})$; see Fig. 2(a). If $\alpha_S \geqslant 0.99$, the transition to a quasiordered magnetic phase is assumed [60]. This situation occurs in two locations of the phase diagram: at the Dirac point ($\delta = 0$) and in the vicinity of the VHS ($\delta = 0.25$). Between these two points, α_S is strong but does not reach the quasiordering criterion. When doping beyond the VHS ($\delta \gtrsim 0.3$), the relative spin fluctuation strength decreases rapidly and the system stays paramagnetic. Increasing the interaction strength amplifies α_S, but the doping dependence remains largely unaffected.

The presence of strong spin fluctuations can induce an effective electron-electron interaction with nonlocal attractive regions, which gives rise to superconducting pairing [88,89]. FLEX captures this effect with the dominant contribution to the effective interaction coming from the spin susceptibility χ^s. Optimal pairing conditions can be inferred from its real-space profile. In Fig. 2(b), we show the doping dependence of up to eighth-nearest-neighbor components of $\chi^s(\mathbf{r})$ for $U/t = 6$. For doping levels in the vicinity of the Dirac point, antiferromagnetic fluctuations with respect to the sublattices A and B emerge, i.e., the AB (intersublattice) components have a negative sign, whereas the AA (intrasublattice) components are positive. Upon doping, initially the longest range and successively the more short-range components of χ^s change their sign. Hence, antiferromagnetic fluctuations are suppressed, and an admixture of ferromagnetic components to χ^s is triggered away from the Dirac point. Beyond the VHS, fluctuations turn increasingly ferromagnetic and their relative strength weakens. Further insight into the emerging SDWs and their origin from nesting conditions can be gained by inspecting the momentum-resolved structure of χ^s [60].

To investigate the dominant superconducting pairing symmetry and transition temperature T_c, we solve the linearized Eliashberg equation for different possible order parameters. In all our calculations, the degenerate singlet d-wave pairings (d_{xy}, $d_{x^2-y^2}$) emerge as the dominant pairing symmetries [60]. This is in agreement with the antiferromagnetic fluctuations as they favor singlet-pairing symmetries. Below T_c, the order parameter forms a time-reversal symmetry-broken chiral $d + id$ pairing state [38,39,69].

In Fig. 3(a), we show the doping dependence of T_c for different U/t. We find a superconducting dome that is characterized by a nonmonotonous behavior with a maximal value $T_c^{\max}$ at an optimal doping δ_{opt}. The existence of such a maximum results from the interplay of the pairing interaction pattern and the electronic DOS at the Fermi level [60]. Doping away from the Dirac point increases the DOS at the Fermi level, which supports d-wave pairing via antiferromagnetic spin fluctuations. As the doping level increases further, however, an increasing amount of pair-breaking ferromagnetic spin fluctuations emerges [cf. Fig. 2(b)]. Thus, we reach a situation of optimal doping around $\delta_{\text{opt}} = 0.06$ and a decrease in T_c upon further doping.

We obtain increasing T_c with increasing interaction U until the highest T_c curve for $U/t = 8$ with a maximal value of $T_c^{\max}/t = 4.8 \times 10^{-3}$ at $\delta_{\text{opt}} = 0.06$ is reached. For larger interactions $U/t \gtrsim 9$, the superconducting transition temperatures decrease again.

Near the VHS, possible superconducting order [39,67,68,90] is masked by magnetic fluctuations in FLEX, that is, α_S exceeds 0.99. As the spin fluctuations turn ferromagnetic towards and beyond the VHS doping, singlet-pairing emerging from antiferromagnetic spin fluctuation exchange is strongly suppressed. In addition, triplet superconductivity does not arise for any temperature $T/t > 10^{-3}$ due to the weakened fluctuation strength [60]. The material and twist-angle-dependent hopping amplitudes given in Fig. 1(c) set the temperature scale. T_c takes values on the order of 0.1–1 K, which is in agreement with reports on other twisted 2D systems [8,9,20,27].

Spin Fluctuations Versus Electron-phonon Coupling. The previous discussion showed that superconductivity arising from a spin-fluctuation-mediated pairing mechanism exhibits a characteristic doping-dependent transition line with a clear maximum near Dirac filling. To contrast this pairing scenario,

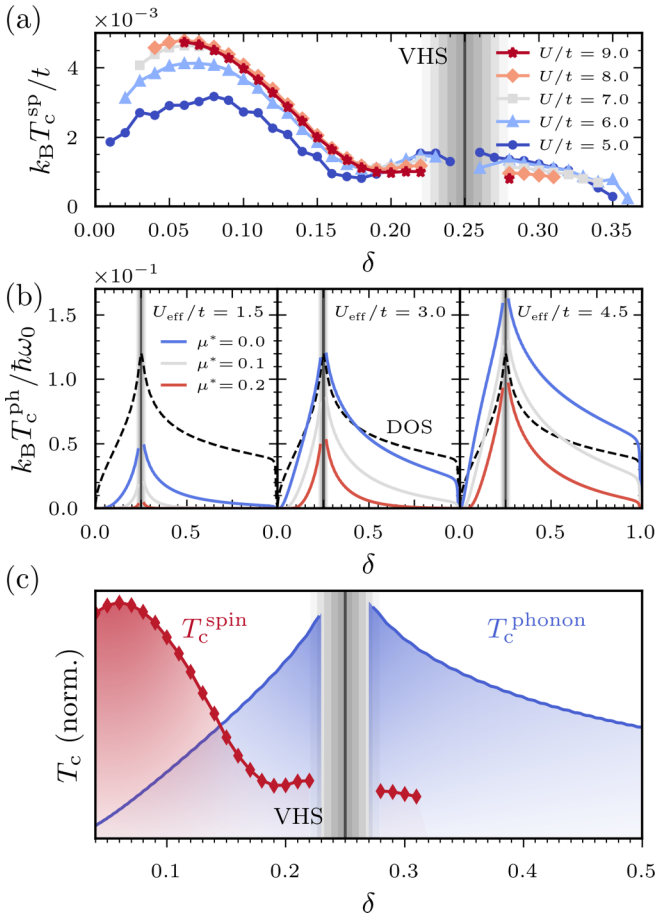

FIG. 3. Doping dependence of the superconducting transition temperature T_c in Γ-valley twisted TMDCs. (a) Phase diagram for spin-fluctuation-mediated pairing for different local Coulomb interaction strengths U/t from FLEX calculations. The critical temperature T_c/t belongs to the dominant singlet d-wave pairing symmetry. (b) Phonon-mediated T_c for an Einstein-Holstein phonon mode ω_0 and for different Coulomb pseudopotentials $\mu^* = 0.0$ (blue), 0.1 (gray), and 0.2 (red). From left to right, the effective attractive interaction U_{eff} from electron-phonon coupling is increased. The trend of the density of states (DOS) is indicated by black dashed lines. (c) Comparison of the doping-dependent phase diagram of the maximum T_c obtained for spin fluctuations and phonons. This phase diagram holds qualitatively for all Γ-valley twisted TMDCs.

we assess how the doping characteristics appear in the conventional case of phonon-mediated superconductivity.

We estimate the transition temperature T_c^{ph} by means of McMillan's formula [91,92]

$$T_c^{ph} = \frac{\hbar\langle\omega\rangle}{1.20\,k_B} \exp\left\{\frac{-1.04(1+\lambda)}{\lambda - 0.62\lambda\mu^* - \mu^*}\right\}, \tag{3}$$

where $\langle\omega\rangle$ is an effective phonon frequency, λ denotes the effective pairing strength, and μ^* is the Tolmachev-Morel-Anderson Coulomb pseudopotential [93,94]. $\langle\omega\rangle$ and λ are generally obtained from the phonon spectral function $\alpha^2F(\omega)$. Here, we consider the limiting case of an Einstein-Holstein phonon mode, i.e., with a constant electron-phonon coupling g and a constant phonon frequency ω_0. We discuss the opposite limit of nonlocal Peierls coupling with dispersive phonons in the Supplemental Material [60].

When discussing phonon-mediated superconductivity, it is simplest to do so in terms of a BCS-like effective attractive interaction U_{eff} such that $\lambda = U_{eff}N(\delta)$ with the DOS $N(\delta)$ per spin and unit cell for a particular doping δ. In the Einstein-Holstein model, we explicitly have $U_{eff} = 2g^2/\hbar\omega_0$ and $\langle\omega\rangle = \omega_0$. The exact values of ω_0, U_{eff}, and μ^* are material-specific and they depend on factors such as twist angle or external screening [95–101]. Twisted TMDCs display phonon modes at energies on the order of a few 10 meV as in the bulk and in addition feature moiré phonons in the range 2–5 meV [100–102]. We estimate U_{eff} to be in the large range of 0.05–8t [60], and typical values of μ^* are in the range 0.0–0.2 [94].

The key observation is that the generic doping dependence of T_c^{ph} derives mainly from the DOS. To illustrate this point, we show in Fig. 3(b) results for T_c^{ph} in units of ω_0 for different U_{eff} and μ^* together with the DOS. We tune U_{eff} to yield weak to intermediate coupling strengths ($\lambda \lesssim 1$). Increasing μ^* suppresses T_c^{ph}, while increasing U_{eff} has the opposite effect. The quantitative details may vary, but the qualitative shape of the T_c^{ph} curve is unaffected in both cases, mainly following $N(\delta)$. Our findings for nonlocal coupling [60] support the robustness of the doping dependence of T_c^{ph}: A peaked structure emerges around the VHS and extends over the whole range of dopings $\delta \in [0, 1]$, i.e., in particular also beyond the VHS in the region of $\delta > 0.25$. The relevant temperature scale is set by ω_0, with T_c^{ph} taking values on the order of 0.1–10 K. Note that we excluded the immediate region around the VHS in our discussion since the competition of different instabilities complicates the determination of the doping dependence [103–105].

A direct comparison of the doping-dependent superconducting phase diagram obtained for the different pairing mechanisms—spin fluctuations and phonons—is given in Fig. 3(c). We use the normalized results of Fig. 3(a) for $U/t = 8$ and those of Fig. 3(b) for $U_{eff}/t = 3$ and $\mu^* = 0.0$. Each pairing mechanism shows unique fingerprints for which we identify two key differences. First, phonon-mediated superconductivity shows a clear increase towards the VHS, whereas for spin-fluctuation-mediated pairing, a global maximum appears close to the Dirac point at δ_{opt}. Second, phonon-induced superconductivity persists over a wider doping range and is closely linked to the DOS, while spin-fluctuation-mediated superconductivity is confined to a narrow doping region near an antiferromagnetic instability, which diminishes rapidly after the VHS due to the emergence of pair-breaking ferromagnetic fluctuations.

Summary and Outlook. We have shown that the superconducting response to doping in Γ-valley twisted TMDCs depends decisively on the quantum nature of the pairing fluctuations. Superconducting pairing mechanisms and their experimental determination present a major open problem in twisted 2D systems. Thus, the question is, are there simple experimental ways to discern different pairing mechanisms?

Our analysis demonstrates that different pairing mechanisms can be distinguished by simple doping-dependent

transport experiments of T_c. Fingerprints unique to the particular microscopic mechanism can be found with respect to the doping levels of maximal T_c or the doping extent over which superconductivity persists.

This possibility has not been explored in other unconventional superconductors [106] because of the difficulties of performing systematic doping-dependent studies. The consideration of multiple local and nonlocal electron-phonon coupling profiles [60] indicates that the distinct doping dependence between T_c^{sp} and T_c^{ph} is generic. Hence, our conclusions are not only valid for the Γ-valley twisted TMDCs, but they can help to elucidate pairing mechanisms in other twisted 2D Van der Waals materials, such as MATBG or MATTG.

Acknowledgments. We acknowledge support and funding by the Deutsche Forschungsgemeinschaft (DFG) via RTG 2247 (QM^3) (Project No. 286518848), via the priority program SPP 2244 (Project No. 422707584), via EXC 2077 (University Allowance, University of Bremen, Project No. 390741603), and via the Cluster of Excellence 'CUI: Advanced Imaging of Matter' – EXC 2056 (Project No. 390715994). Funding from the European Commission via the Graphene Flagship Core Project 3 (Grant Agreement ID: 881603) and computing time at the HLRN facilities (Berlin and Göttingen) are acknowledged. This work was supported by a Grant-in-Aid for Scientific Research (No. 19H05825) by MEXT and by JST PRESTO (No. JPMJPR20L7), Japan.

[1] E. Suárez Morell, J. D. Correa, P. Vargas, M. Pacheco, and Z. Barticevic, Flat bands in slightly twisted bilayer graphene: Tight-binding calculations, Phys. Rev. B **82**, 121407(R) (2010).

[2] R. Bistritzer and A. H. MacDonald, Moiré bands in twisted double-layer graphene, Proc. Natl. Acad. Sci. (USA) **108**, 12233 (2011).

[3] M. Koshino, N. F. Q. Yuan, T. Koretsune, M. Ochi, K. Kuroki, and L. Fu, Maximally Localized Wannier Orbitals and the Extended Hubbard Model for Twisted Bilayer Graphene, Phys. Rev. X **8**, 031087 (2018).

[4] A. Marrazzo, M. Gibertini, D. Campi, N. Mounet, and N. Marzari, Prediction of a Large-Gap and Switchable Kane-Mele Quantum Spin Hall Insulator, Phys. Rev. Lett. **120**, 117701 (2018).

[5] X. Wu, M. Fink, W. Hanke, R. Thomale, and D. Di Sante, Unconventional superconductivity in a doped quantum spin Hall insulator, Phys. Rev. B **100**, 041117(R) (2019).

[6] J. M. Pizarro, S. Adler, K. Zantout, T. Mertz, P. Barone, R. Valentí, G. Sangiovanni, and T. O. Wehling, Deconfinement of Mott localized electrons into topological and spin-orbit-coupled Dirac fermions, npj Quantum Mater. **5**, 79 (2020).

[7] Y. Cao, V. Fatemi, A. Demir, S. Fang, S. L. Tomarken, J. Y. Luo, J. D. Sanchez-Yamagishi, K. Watanabe, T. Taniguchi, E. Kaxiras, R. C. Ashoori, and P. Jarillo-Herrero, Correlated insulator behaviour at half-filling in magic-angle graphene superlattices, Nature (London) **556**, 80 (2018).

[8] Y. Cao, V. Fatemi, S. Fang, K. Watanabe, T. Taniguchi, E. Kaxiras, and P. Jarillo-Herrero, Unconventional superconductivity in magic-angle graphene superlattices, Nature (London) **556**, 43 (2018).

[9] M. Yankowitz, S. Chen, H. Polshyn, Y. Zhang, K. Watanabe, T. Taniguchi, D. Graf, A. F. Young, and C. R. Dean, Tuning superconductivity in twisted bilayer graphene, Science **363**, 1059 (2019).

[10] G. Chen, L. Jiang, S. Wu, B. Lyu, H. Li, B. L. Chittari, K. Watanabe, T. Taniguchi, Z. Shi, J. Jung, Y. Zhang, and F. Wang, Evidence of a gate-tunable Mott insulator in a trilayer graphene moiré superlattice, Nat. Phys. **15**, 237 (2019).

[11] A. L. Sharpe, E. J. Fox, A. W. Barnard, J. Finney, K. Watanabe, T. Taniguchi, M. A. Kastner, and D. Goldhaber-Gordon, Emergent ferromagnetism near three-quarters filling in twisted bilayer graphene, Science **365**, 605 (2019).

[12] X. Lu, P. Stepanov, W. Yang, M. Xie, M. A. Aamir, I. Das, C. Urgell, K. Watanabe, T. Taniguchi, G. Zhang, A. Bachtold, A. H. MacDonald, and D. K. Efetov, Superconductors, orbital magnets and correlated states in magic-angle bilayer graphene, Nature (London) **574**, 653 (2019).

[13] G. W. Burg, J. Zhu, T. Taniguchi, K. Watanabe, A. H. MacDonald, and E. Tutuc, Correlated Insulating States in Twisted Double Bilayer Graphene, Phys. Rev. Lett. **123**, 197702 (2019).

[14] E. C. Regan, D. Wang, C. Jin, M. I. Bakti Utama, B. Gao, X. Wei, S. Zhao, W. Zhao, Z. Zhang, K. Yumigeta, M. Blei, J. D. Carlström, K. Watanabe, T. Taniguchi, S. Tongay, M. Crommie, A. Zettl, and F. Wang, Mott and generalized Wigner crystal states in WSe_2/WS_2 moiré superlattices, Nature (London) **579**, 359 (2020).

[15] Y. Tang, L. Li, T. Li, Y. Xu, S. Liu, K. Barmak, K. Watanabe, T. Taniguchi, A. H. MacDonald, J. Shan, and K. F. Mak, Simulation of Hubbard model physics in WSe_2/WS_2 moiré superlattices, Nature (London) **579**, 353 (2020).

[16] C. Shen, Y. Chu, Q. Wu, N. Li, S. Wang, Y. Zhao, J. Tang, J. Liu, J. Tian, K. Watanabe, T. Taniguchi, R. Yang, Z. Y. Meng, D. Shi, O. V. Yazyev, and G. Zhang, Correlated states in twisted double bilayer graphene, Nat. Phys. **16**, 520 (2020).

[17] P. Stepanov, I. Das, X. Lu, A. Fahimniya, K. Watanabe, T. Taniguchi, F. H. L. Koppens, J. Lischner, L. Levitov, and D. K. Efetov, Untying the insulating and superconducting orders in magic-angle graphene, Nature (London) **583**, 375 (2020).

[18] Y. Saito, J. Ge, K. Watanabe, T. Taniguchi, and A. F. Young, Independent superconductors and correlated insulators in twisted bilayer graphene, Nat. Phys. **16**, 926 (2020).

[19] Y. Cao, D. Rodan-Legrain, O. Rubies-Bigorda, J. M. Park, K. Watanabe, T. Taniguchi, and P. Jarillo-Herrero, Tunable correlated states and spin-polarized phases in twisted bilayer-bilayer graphene, Nature (London) **583**, 215 (2020).

[20] L. Wang, E.-M. Shih, A. Ghiotto, L. Xian, D. A. Rhodes, C. Tan, M. Claassen, D. M. Kennes, Y. Bai, B. Kim, K. Watanabe, T. Taniguchi, X. Zhu, J. Hone, A. Rubio, A. N. Pasupathy, and C. R. Dean, Correlated electronic phases in twisted bilayer transition metal dichalcogenides, Nat. Mater. **19**, 861 (2020).

[21] S. Chen, M. He, Y.-H. Zhang, V. Hsieh, Z. Fei, K. Watanabe, T. Taniguchi, D. H. Cobden, X. Xu, C. R. Dean, and M. Yankowitz, Electrically tunable correlated and topological states in twisted monolayer–bilayer graphene, Nat. Phys. **17**, 374 (2021).

[22] H. Polshyn, J. Zhu, M. A. Kumar, Y. Zhang, F. Yang, C. L. Tschirhart, M. Serlin, K. Watanabe, T. Taniguchi, A. H. MacDonald, and A. F. Young, Electrical switching of magnetic order in an orbital Chern insulator, Nature (London) **588**, 66 (2020).

[23] K. P. Nuckolls, M. Oh, D. Wong, B. Lian, K. Watanabe, T. Taniguchi, B. A. Bernevig, and A. Yazdani, Strongly correlated Chern insulators in magic-angle twisted bilayer graphene, Nature (London) **588**, 610 (2020).

[24] J. M. Park, Y. Cao, K. Watanabe, T. Taniguchi, and P. Jarillo-Herrero, Tunable strongly coupled superconductivity in magic-angle twisted trilayer graphene, Nature (London) **590**, 249 (2021).

[25] S. Wu, Z. Zhang, K. Watanabe, T. Taniguchi, and E. Y. Andrei, Chern insulators, van Hove singularities and topological flat bands in magic-angle twisted bilayer graphene, Nat. Mater. **20**, 488 (2021).

[26] S. Xu, M. M. Al Ezzi, N. Balakrishnan, A. Garcia-Ruiz, B. Tsim, C. Mullan, J. Barrier, N. Xin, B. A. Piot, T. Taniguchi, K. Watanabe, A. Carvalho, A. Mishchenko, A. K. Geim, V. I. Fal'ko, S. Adam, A. H. C. Neto, K. S. Novoselov, and Y. Shi, Tunable van Hove singularities and correlated states in twisted monolayer-bilayer graphene, Nat. Phys. **17**, 619 (2021).

[27] Y. Cao, D. Rodan-Legrain, J. M. Park, N. F. Q. Yuan, K. Watanabe, T. Taniguchi, R. M. Fernandes, L. Fu, and P. Jarillo-Herrero, Nematicity and competing orders in superconducting magic-angle graphene, Science **372**, 264 (2021).

[28] X. Liu, Z. Wang, K. Watanabe, T. Taniguchi, O. Vafek, and J. I. A. Li, Tuning electron correlation in magic-angle twisted bilayer graphene using Coulomb screening, Science **371**, 1261 (2021).

[29] Y. Cao, J. Y. Luo, V. Fatemi, S. Fang, J. D. Sanchez-Yamagishi, K. Watanabe, T. Taniguchi, E. Kaxiras, and P. Jarillo-Herrero, Superlattice-Induced Insulating States and Valley-Protected Orbits in Twisted Bilayer Graphene, Phys. Rev. Lett. **117**, 116804 (2016).

[30] C.-C. Liu, L.-D. Zhang, W.-Q. Chen, and F. Yang, Chiral Spin Density Wave and $d + id$ Superconductivity in the Magic-Angle-Twisted Bilayer Graphene, Phys. Rev. Lett. **121**, 217001 (2018).

[31] Y.-Z. You and A. Vishwanath, Superconductivity from valley fluctuations and approximate SO(4) symmetry in a weak coupling theory of twisted bilayer graphene, npj Quantum Mater. **4**, 16 (2019).

[32] L. Klebl and C. Honerkamp, Inherited and flatband-induced ordering in twisted graphene bilayers, Phys. Rev. B **100**, 155145 (2019).

[33] A. Fischer, L. Klebl, C. Honerkamp, and D. M. Kennes, Spin-fluctuation-induced pairing in twisted bilayer graphene, Phys. Rev. B **103**, L041103 (2021).

[34] A. Fischer, Z. A. H. Goodwin, A. A. Mostofi, J. Lischner, D. M. Kennes, and L. Klebl, Unconventional superconductivity in magic-angle twisted trilayer graphene, npj Quantum Mater. **7**, 5 (2022).

[35] M. Oh, K. P. Nuckolls, D. Wong, R. L. Lee, X. Liu, K. Watanabe, T. Taniguchi, and A. Yazdani, Evidence for unconventional superconductivity in twisted bilayer graphene, Nature (London) **600**, 240 (2021).

[36] E. F. Talantsev, R. C. Mataira, and W. P. Crump, Classifying superconductivity in moiré graphene superlattices, Sci. Rep. **10**, 212 (2020).

[37] D. M. Kennes, M. Claassen, L. Xian, A. Georges, A. J. Millis, J. Hone, C. R. Dean, D. N. Basov, A. N. Pasupathy, and A. Rubio, Moiré heterostructures as a condensed-matter quantum simulator, Nat. Phys. **17**, 155 (2021).

[38] Z. Kuznetsova and V. Barzykin, Pairing state in multicomponent superconductors, Europhys. Lett. **72**, 437 (2005).

[39] A. M. Black-Schaffer and C. Honerkamp, Chiral d-wave superconductivity in doped graphene, J. Phys.: Condens. Matter **26**, 423201 (2014).

[40] H. C. Po, L. Zou, A. Vishwanath, and T. Senthil, Origin of Mott Insulating Behavior and Superconductivity in Twisted Bilayer Graphene, Phys. Rev. X **8**, 031089 (2018).

[41] J. Y. Lee, E. Khalaf, S. Liu, X. Liu, Z. Hao, P. Kim, and A. Vishwanath, Theory of correlated insulating behaviour and spin-triplet superconductivity in twisted double bilayer graphene, Nat. Commun. **10**, 5333 (2019).

[42] F. Haddadi, Q. Wu, A. J. Kruchkov, and O. V. Yazyev, Moiré flat bands in twisted double bilayer graphene, Nano Lett. **20**, 2410 (2020).

[43] X. Liang, Z. A. H. Goodwin, V. Vitale, F. Corsetti, A. A. Mostofi, and J. Lischner, Effect of bilayer stacking on the atomic and electronic structure of twisted double bilayer graphene, Phys. Rev. B **102**, 155146 (2020).

[44] S. Carr, C. Li, Z. Zhu, E. Kaxiras, S. Sachdev, and A. Kruchkov, Ultraheavy and ultrarelativistic Dirac quasiparticles in sandwiched graphenes, Nano Lett. **20**, 3030 (2020).

[45] Z. Wu, Z. Zhan, and S. Yuan, Lattice relaxation, mirror symmetry and magnetic field effects on ultraflat bands in twisted trilayer graphene, Sci. China Phys. Mech. Astron. **64**, 267811 (2021).

[46] A. Lopez-Bezanilla and J. L. Lado, Electrical band flattening, valley flux, and superconductivity in twisted trilayer graphene, Phys. Rev. Res. **2**, 033357 (2020).

[47] L. Xian, D. M. Kennes, N. Tancogne-Dejean, M. Altarelli, and A. Rubio, Multiflat bands and strong correlations in twisted bilayer boron nitride: Doping-induced correlated insulator and superconductor, Nano Lett. **19**, 4934 (2019).

[48] L. Xian, M. Claassen, D. Kiese, M. M. Scherer, S. Trebst, D. M. Kennes, and A. Rubio, Realization of nearly dispersionless bands with strong orbital anisotropy from destructive interference in twisted bilayer MoS_2, Nat. Commun. **12**, 5644 (2021).

[49] M. Angeli and A. H. MacDonald, Γ valley transition metal dichalcogenide moiré bands, Proc. Natl. Acad. Sci. (USA) **118**, e2021826118 (2021).

[50] H. C. Po, L. Zou, T. Senthil, and A. Vishwanath, Faithful tight-binding models and fragile topology of magic-angle bilayer graphene, Phys. Rev. B **99**, 195455 (2019).

[51] S. Carr, S. Fang, Z. Zhu, and E. Kaxiras, Exact continuum model for low-energy electronic states of twisted bilayer graphene, Phys. Rev. Res. **1**, 013001 (2019).

[52] V. o. T. Phong and E. J. Mele, Obstruction and Interference in Low-Energy Models for Twisted Bilayer Graphene, Phys. Rev. Lett. **125**, 176404 (2020).

[53] L. Zou, H. C. Po, A. Vishwanath, and T. Senthil, Band structure of twisted bilayer graphene: Emergent symmetries, commensurate approximants, and Wannier obstructions, Phys. Rev. B **98**, 085435 (2018).

[54] N. E. Bickers, D. J. Scalapino, and S. R. White, Conserving Approximations for Strongly Correlated Electron Systems: Bethe-Salpeter Equation and Dynamics for the Two-Dimensional Hubbard Model, Phys. Rev. Lett. **62**, 961 (1989).

[55] N. E. Bickers and D. J. Scalapino, Conserving approximations for strongly fluctuating electron systems. I. Formalism and calculational approach, Ann. Phys. **193**, 206 (1989).

[56] Y. Zhang, N. F. Q. Yuan, and L. Fu, Moiré quantum chemistry: Charge transfer in transition metal dichalcogenide superlattices, Phys. Rev. B **102**, 201115(R) (2020).

[57] Y. Zhang, T. Liu, and L. Fu, Electronic structures, charge transfer, and charge order in twisted transition metal dichalcogenide bilayers, Phys. Rev. B **103**, 155142 (2021).

[58] F. A. Rasmussen and K. S. Thygesen, Computational 2D materials database: Electronic structure of transition-metal dichalcogenides and oxides, J. Phys. Chem. C **119**, 13169 (2015).

[59] A. Chaves, J. G. Azadani, H. Alsalman, D. R. da Costa, R. Frisenda, A. J. Chaves, S. H. Song, Y. D. Kim, D. He, J. Zhou, A. Castellanos-Gomez, F. M. Peeters, Z. Liu, C. L. Hinkle, S.-H. Oh, P. D. Ye, S. J. Koester, Y. H. Lee, P. Avouris, X. Wang *et al.*, Bandgap engineering of two-dimensional semiconductor materials, npj 2D Mater. Appl. **4**, 29 (2020).

[60] See Supplemental Material at http://link.aps.org/supplemental/10.1103/PhysRevB.105.L241109 for details on the low-energy continuum model of the electronic bands in Γ-valley twisted TMDCs, for the construction of the Wannier orbitals in the 2D honeycomb moiré pattern, for a study of the electrostatic and long-range Hartree potential in the flat Dirac bands, for an estimation of the on-site and nearest-neighbor Coulomb interaction, for numerical details on the FLEX calculations, for a discussion on the nature of magnetic ordering, for an in-depth discussion of the spin susceptibility structure, for the temperature dependence of the d- and f-wave superconducting eigenvalues and order parameters, for a discussion of the influence of band asymmetry as induced by long-range hopping, for a study of superconductivity arising from nonlocal dispersive phonons, and for an estimation of the phonon-induced attractive interaction U_{eff} and it includes Refs. [17,18,28,34,38,39,49,54,55,61–64,68,69,73–77,80,81,83,91,104,107–137].

[61] F. Guinea and N. R. Walet, Electrostatic effects, band distortions, and superconductivity in twisted graphene bilayers, Proc. Natl. Acad. Sci. (USA) **115**, 13174 (2018).

[62] T. Cea, N. R. Walet, and F. Guinea, Electronic band structure and pinning of Fermi energy to Van Hove singularities in twisted bilayer graphene: A self-consistent approach, Phys. Rev. B **100**, 205113 (2019).

[63] T. Cea and F. Guinea, Band structure and insulating states driven by Coulomb interaction in twisted bilayer graphene, Phys. Rev. B **102**, 045107 (2020).

[64] M. J. Calderón and E. Bascones, Interactions in the 8-orbital model for twisted bilayer graphene, Phys. Rev. B **102**, 155149 (2020).

[65] A. H. Castro Neto, F. Guinea, N. M. R. Peres, K. S. Novoselov, and A. K. Geim, The electronic properties of graphene, Rev. Mod. Phys. **81**, 109 (2009).

[66] F. F. Assaad and I. F. Herbut, Pinning the Order: The Nature of Quantum Criticality in the Hubbard Model on Honeycomb Lattice, Phys. Rev. X **3**, 031010 (2013).

[67] M. L. Kiesel, C. Platt, W. Hanke, D. A. Abanin, and R. Thomale, Competing many-body instabilities and unconventional superconductivity in graphene, Phys. Rev. B **86**, 020507(R) (2012).

[68] W.-S. Wang, Y.-Y. Xiang, Q.-H. Wang, F. Wang, F. Yang, and D.-H. Lee, Functional renormalization group and variational Monte Carlo studies of the electronic instabilities in graphene near $\frac{1}{4}$ doping, Phys. Rev. B **85**, 035414 (2012).

[69] R. Nandkishore, L. S. Levitov, and A. V. Chubukov, Chiral superconductivity from repulsive interactions in doped graphene, Nat. Phys. **8**, 158 (2012).

[70] X. Y. Xu, S. Wessel, and Z. Y. Meng, Competing pairing channels in the doped honeycomb lattice Hubbard model, Phys. Rev. B **94**, 115105 (2016).

[71] M. Raczkowski, R. Peters, T. T. Phùng, N. Takemori, F. F. Assaad, A. Honecker, and J. Vahedi, Hubbard model on the honeycomb lattice: From static and dynamical mean-field theories to lattice quantum Monte Carlo simulations, Phys. Rev. B **101**, 125103 (2020).

[72] N. C. Costa, K. Seki, and S. Sorella, Magnetism and Charge Order in the Honeycomb Lattice, Phys. Rev. Lett. **126**, 107205 (2021).

[73] K. Kuroki and R. Arita, Spin-triplet superconductivity in repulsive Hubbard models with disconnected Fermi surfaces: A case study on triangular and honeycomb lattices, Phys. Rev. B **63**, 174507 (2001).

[74] S. Onari, K. Kuroki, R. Arita, and H. Aoki, Superconductivity induced by interband nesting in the three-dimensional honeycomb lattice, Phys. Rev. B **65**, 184525 (2002).

[75] K. Kuroki, Spin-fluctuation-mediated $d + id'$ pairing mechanism in doped β-MNCl (M=Hf,Zr) superconductors, Phys. Rev. B **81**, 104502 (2010).

[76] J. Li, M. Wallerberger, N. Chikano, C.-N. Yeh, E. Gull, and H. Shinaoka, Sparse sampling approach to efficient ab initio calculations at finite temperature, Phys. Rev. B **101**, 035144 (2020).

[77] N. Witt, E. G. C. P. van Loon, T. Nomoto, R. Arita, and T. O. Wehling, Efficient fluctuation-exchange approach to low-temperature spin fluctuations and superconductivity: From the Hubbard model to $Na_xCoO_2 \cdot yH_2O$, Phys. Rev. B **103**, 205148 (2021).

[78] M. Rösner, C. Steinke, M. Lorke, C. Gies, F. Jahnke, and T. O. Wehling, Two-dimensional heterojunctions from nonlocal manipulations of the interactions, Nano Lett. **16**, 2322 (2016).

[79] A. Raja, A. Chaves, J. Yu, G. Arefe, H. M. Hill, A. F. Rigosi, T. C. Berkelbach, P. Nagler, C. Schüller, T. Korn, C. Nuckolls, J. Hone, L. E. Brus, T. F. Heinz, D. R. Reichman, and A. Chernikov, Coulomb engineering of the bandgap and excitons in two-dimensional materials, Nat. Commun. **8**, 15251 (2017).

[80] J. M. Pizarro, M. Rösner, R. Thomale, R. Valentí, and T. O. Wehling, Internal screening and dielectric engineering

in magic-angle twisted bilayer graphene, Phys. Rev. B **100**, 161102(R) (2019).

[81] Z. A. H. Goodwin, F. Corsetti, A. A. Mostofi, and J. Lischner, Twist-angle sensitivity of electron correlations in moiré graphene bilayers, Phys. Rev. B **100**, 121106(R) (2019).

[82] Z. A. H. Goodwin, V. Vitale, F. Corsetti, D. K. Efetov, A. A. Mostofi, and J. Lischner, Critical role of device geometry for the phase diagram of twisted bilayer graphene, Phys. Rev. B **101**, 165110 (2020).

[83] H. S. Arora, R. Polski, Y. Zhang, A. Thomson, Y. Choi, H. Kim, Z. Lin, I. Z. Wilson, X. Xu, J.-H. Chu, K. Watanabe, T. Taniguchi, J. Alicea, and S. Nadj-Perge, Superconductivity in metallic twisted bilayer graphene stabilized by WSe_2, Nature (London) **583**, 379 (2020).

[84] M. Kim, S. G. Xu, A. I. Berdyugin, A. Principi, S. Slizovskiy, N. Xin, P. Kumaravadivel, W. Kuang, M. Hamer, R. K. Kumar, R. V. Gorbachev, K. Watanabe, T. Taniguchi, I. V. Grigorieva, V. I. Fal'ko, M. Polini, and A. K. Geim, Control of electron-electron interaction in graphene by proximity screening, Nat. Commun. **11**, 2339 (2020).

[85] N. Bulut, D. J. Scalapino, and S. R. White, Comparison of Monte Carlo and diagrammatic calculations for the two-dimensional Hubbard model, Phys. Rev. B **47**, 2742 (1993).

[86] N. Bulut, D. J. Scalapino, and S. R. White, Effective electron-electron interaction in the two-dimensional Hubbard model, Phys. Rev. B **50**, 9623 (1994).

[87] J. Zhang, R. Sknepnek, R. M. Fernandes, and J. Schmalian, Orbital coupling and superconductivity in the iron pnictides, Phys. Rev. B **79**, 220502(R) (2009).

[88] T. Moriya and K. Ueda, Antiferromagnetic spin fluctuation and superconductivity, Rep. Prog. Phys. **66**, 1299 (2003).

[89] D. J. Scalapino, A common thread: The pairing interaction for unconventional superconductors, Rev. Mod. Phys. **84**, 1383 (2012).

[90] T. Ying and S. Wessel, Pairing and chiral spin density wave instabilities on the honeycomb lattice: A comparative quantum Monte Carlo study, Phys. Rev. B **97**, 075127 (2018).

[91] W. L. McMillan, Transition temperature of strong-coupled superconductors, Phys. Rev. **167**, 331 (1968).

[92] R. Dynes, McMillan's equation and the T_c of superconductors, Solid State Commun. **10**, 615 (1972).

[93] V. V. Tolmachev, Logarithmic criterion for superconductivity, Dokl. Akad. Nauk SSSR **140**, 563 (1961).

[94] P. Morel and P. W. Anderson, Calculation of the superconducting state parameters with retarded electron-phonon interaction, Phys. Rev. **125**, 1263 (1962).

[95] F. Wu, A. H. MacDonald, and I. Martin, Theory of Phonon-Mediated Superconductivity in Twisted Bilayer Graphene, Phys. Rev. Lett. **121**, 257001 (2018).

[96] M.-L. Lin, Q.-H. Tan, J.-B. Wu, X.-S. Chen, J.-H. Wang, Y.-H. Pan, X. Zhang, X. Cong, J. Zhang, W. Ji, P.-A. Hu, K.-H. Liu, and P.-H. Tan, Moiré phonons in twisted bilayer MoS_2, ACS Nano Nano **12**, 8770 (2018).

[97] Y. W. Choi and H. J. Choi, Strong electron-phonon coupling, electron-hole asymmetry, and nonadiabaticity in magic-angle twisted bilayer graphene, Phys. Rev. B **98**, 241412(R) (2018).

[98] B. Lian, Z. Wang, and B. A. Bernevig, Twisted Bilayer Graphene: A Phonon-Driven Superconductor, Phys. Rev. Lett. **122**, 257002 (2019).

[99] R. Debnath, I. Maity, R. Biswas, V. Raghunathan, M. Jain, and A. Ghosh, Evolution of high-frequency Raman modes and their doping dependence in twisted bilayer MoS_2, Nanoscale **12**, 17272 (2020).

[100] K.-Q. Lin, J. Holler, J. M. Bauer, P. Parzefall, M. Scheuck, B. Peng, T. Korn, S. Bange, J. M. Lupton, and C. Schüller, Large-scale mapping of moiré superlattices by hyperspectral Raman imaging, Adv. Mater. **33**, 2008333 (2021).

[101] P. Parzefall, J. Holler, M. Scheuck, A. Beer, K.-Q. Lin, B. Peng, B. Monserrat, P. Nagler, M. Kempf, T. Korn, and C. Schüller, Moiré phonons in twisted $MoSe_2$–WSe_2 heterobilayers and their correlation with interlayer excitons, 2D Mater. **8**, 035030 (2021).

[102] J. Quan, L. Linhart, M.-L. Lin, D. Lee, J. Zhu, C.-Y. Wang, W.-T. Hsu, J. Choi, J. Embley, C. Young, T. Taniguchi, K. Watanabe, C.-K. Shih, K. Lai, A. H. MacDonald, P.-H. Tan, F. Libisch, and X. Li, Phonon renormalization in reconstructed MoS_2 moiré superlattices, Nat. Mater. **20**, 1100 (2021).

[103] T. M. Rice and G. K. Scott, New Mechanism for a Charge-Density-Wave Instability, Phys. Rev. Lett. **35**, 120 (1975).

[104] S. Jiang, A. Mesaros, and Y. Ran, Chiral Spin-Density Wave, Spin-Charge-Chern Liquid, and $d + id$ Superconductivity in 1/4-Doped Correlated Electronic Systems on the Honeycomb Lattice, Phys. Rev. X **4**, 031040 (2014).

[105] J. Berges, E. G. C. P. van Loon, A. Schobert, M. Rösner, and T. O. Wehling, *Ab initio* phonon self-energies and fluctuation diagnostics of phonon anomalies: Lattice instabilities from Dirac pseudospin physics in transition metal dichalcogenides, Phys. Rev. B **101**, 155107 (2020).

[106] B. Keimer, S. A. Kivelson, M. R. Norman, S. Uchida, and J. Zaanen, From quantum matter to high-temperature superconductivity in copper oxides, Nature (London) **518**, 179 (2015).

[107] D. Xiao, G.-B. Liu, W. Feng, X. Xu, and W. Yao, Coupled Spin and Valley Physics in Monolayers of MoS_2 and Other Group-VI Dichalcogenides, Phys. Rev. Lett. **108**, 196802 (2012).

[108] S. Venkateswarlu, A. Honecker, and G. Trambly de Laissardière, Electronic localization in twisted bilayer mos_2 with small rotation angle, Phys. Rev. B **102**, 081103(R) (2020).

[109] N. Marzari, A. A. Mostofi, J. R. Yates, I. Souza, and D. Vanderbilt, Maximally localized Wannier functions: Theory and applications, Rev. Mod. Phys. **84**, 1419 (2012).

[110] N. F. Q. Yuan, H. Isobe, and L. Fu, Magic of high-order van Hove singularity, Nat. Commun. **10**, 5769 (2019).

[111] L. Classen, A. V. Chubukov, C. Honerkamp, and M. M. Scherer, Competing orders at higher-order Van Hove points, Phys. Rev. B **102**, 125141 (2020).

[112] G. P. Kerker, Efficient iteration scheme for self-consistent pseudopotential calculations, Phys. Rev. B **23**, 3082 (1981).

[113] E. G. C. P. van Loon, M. Schüler, M. I. Katsnelson, and T. O. Wehling, Capturing nonlocal interaction effects in the Hubbard model: Optimal mappings and limits of applicability, Phys. Rev. B **94**, 165141 (2016).

[114] K. Ohno, Some remarks on the Pariser-Parr-Pople method, Theor. Chim. Acta **2**, 219 (1964).

[115] T. Cea and F. Guinea, Coulomb interaction, phonons, and superconductivity in twisted bilayer graphene, Proc. Natl. Acad. Sci. (USA) **118**, e2107874118 (2021).

[116] A. Laturia, M. L. Van de Put, and W. G. Vandenberghe, Dielectric properties of hexagonal boron nitride and transition metal

dichalcogenides: from monolayer to bulk, npj 2D Mater. Appl. **2**, 6 (2018).

[117] A. Weston, Y. Zou, V. Enaldiev, A. Summerfield, N. Clark, V. Zólyomi, A. Graham, C. Yelgel, S. Magorrian, M. Zhou, J. Zultak, D. Hopkinson, A. Barinov, T. H. Bointon, A. Kretinin, N. R. Wilson, P. H. Beton, V. I. Fal'ko, S. J. Haigh, and R. Gorbachev, Atomic reconstruction in twisted bilayers of transition metal dichalcogenides, Nat. Nanotechnol. **15**, 592 (2020).

[118] H. Kontani and K. Ueda, Electronic Properties of the Trellis-Lattice Hubbard Model: Pseudogap and Superconductivity, Phys. Rev. Lett. **80**, 5619 (1998).

[119] S. Koikegami, S. Fujimoto, and K. Yamada, Electronic structure and transition temperature of the d-p model, J. Phys. Soc. Jpn. **66**, 1438 (1997).

[120] H. Shinaoka, N. Chikano, E. Gull, J. Li, T. Nomoto, J. Otsuki, M. Wallerberger, T. Wang, and K. Yoshimi, arXiv:2106.12685.

[121] H. Shinaoka, J. Otsuki, M. Ohzeki, and K. Yoshimi, Compressing Green's function using intermediate representation between imaginary-time and real-frequency domains, Phys. Rev. B **96**, 035147 (2017).

[122] N. Chikano, K. Yoshimi, J. Otsuki, and H. Shinaoka, irbasis: Open-source database and software for intermediate-representation basis functions of imaginary-time Green's function, Comput. Phys. Commun. **240**, 181 (2019).

[123] M. Sigrist and K. Ueda, Phenomenological theory of unconventional superconductivity, Rev. Mod. Phys. **63**, 239 (1991).

[124] N. D. Mermin and H. Wagner, Absence of Ferromagnetism or Antiferromagnetism in One- or Two-Dimensional Isotropic Heisenberg Models, Phys. Rev. Lett. **17**, 1307 (1966).

[125] H. Kontani and M. Ohno, Effect of a nonmagnetic impurity in a nearly antiferromagnetic Fermi liquid: Magnetic correlations and transport phenomena, Phys. Rev. B **74**, 014406 (2006).

[126] H. Kino and H. Kontani, Phase diagram of superconductivity on the anisotropic triangular lattice Hubbard model: An effective model of κ-(BEDT-TTF) salts, J. Phys. Soc. Jpn. **67**, 3691 (1998).

[127] M. Kitatani, N. Tsuji, and H. Aoki, FLEX+DMFT approach to the d-wave superconducting phase diagram of the two-dimensional Hubbard model, Phys. Rev. B **92**, 085104 (2015).

[128] W. A. Harrison, *Elementary Electronic Structure*, rev. ed. (World Scientific, Singapore, 2004).

[129] P. B. Allen and R. C. Dynes, Transition temperature of strong-coupled superconductors reanalyzed, Phys. Rev. B **12**, 905 (1975).

[130] M. Rösner, S. Haas, and T. O. Wehling, Phase diagram of electron-doped dichalcogenides, Phys. Rev. B **90**, 245105 (2014).

[131] G. Schönhoff, M. Rösner, R. E. Groenewald, S. Haas, and T. O. Wehling, Interplay of screening and superconductivity in low-dimensional materials, Phys. Rev. B **94**, 134504 (2016).

[132] G. D. Mahan, *Many-Particle Physics*, 3rd ed. (Springer, US, 2000).

[133] J. L. Feldman, Elastic constants of 2H-MoS_2 and 2H-$NbSe_2$ extracted from measured dispersion curves and linear compressibilities, J. Phys. Chem. Solids **37**, 1141 (1976).

[134] Y. Zhao, X. Luo, H. Li, J. Zhang, P. T. Araujo, C. K. Gan, J. Wu, H. Zhang, S. Y. Quek, M. S. Dresselhaus, and Q. Xiong, Interlayer breathing and shear modes in few-trilayer MoS_2 and WSe_2, Nano Lett. **13**, 1007 (2013).

[135] L. D. Landau and E. M. Lifshitz, *Theory of Elasticity*, 2nd ed. (Pergamon, Oxford, 1970), Vol. 7.

[136] D. Çakır, F. M. Peeters, and C. Sevik, Mechanical and thermal properties of h-MX_2 (M=Cr, Mo, W; X=O, S, Se, Te) monolayers: A comparative study, Appl. Phys. Lett. **104**, 203110 (2014).

[137] K. Liu, Q. Yan, M. Chen, W. Fan, Y. Sun, J. Suh, D. Fu, S. Lee, J. Zhou, S. Tongay, J. Ji, J. B. Neaton, and J. Wu, Elastic properties of chemical-vapor-deposited monolayer MoS_2, WS_2, and their bilayer heterostructures, Nano Lett. **14**, 5097 (2014).